



# CHORUS

This is the accepted manuscript made available via CHORUS. The article has been published as:

## Control of Rydberg-atom blockade by dc electric-field orientation in a quasi-one-dimensional sample

Luís Felipe Gonçalves and Luis Gustavo Marcassa

Phys. Rev. A **94**, 043424 — Published 28 October 2016

DOI: [10.1103/PhysRevA.94.043424](https://doi.org/10.1103/PhysRevA.94.043424)

# Control of Rydberg atom blockade by dc electric field orientation in a quasi-unidimensional sample

Luís Felipe Gonçalves and Luis Gustavo Marcassa  
*Instituto de Física de São Carlos, Universidade de São Paulo,  
Caixa Postal 369, 13560-970, São Carlos, SP, Brasil*

Rydberg atoms possess a strong atom-atom interaction, which limits its density in an atomic sample. Such effect is known as Rydberg atom blockade. Here, we present a novel way to control such effect by directly orienting the induced atomic dipole moment using a dc external electrical field. To demonstrate it, we excite the  $50S_{1/2}$  Rb atomic state in a quasi-unidimensional sample held in a quasi-electrostatic trap. A pure  $nS$  state holds only van der Waals interaction at long range, but in the presence of an external electric field the state mixing leads to strong dipole-dipole interactions. We have measured the Rydberg atom population as a function of ground state atoms density for several angles between the electric field and the main axis of the unidimensional sample. The results indicate that the limit on the final Rydberg density can be controlled by electric field orientation. Besides, we have characterized the sample by using a single-atom ion imaging technique, demonstrating that it does behave as an unidimensional sample.

Rydberg atom interactions play a key role on the study of very intrinsic properties of cold matter [1]. It helps us to understand long-range interactions [2, 3], atomic collisions [2, 4, 5], molecular formation [6] and also macroscopic manifestation of atomic phenomena like van der Waals and dipole-dipole interactions [7, 8]. Besides, they are essential for the development of quantum computation [9] and the study of coherent systems [10]. Such systems rely on the Rydberg atom blockade effect [11–13], which is a density limitation of Rydberg atomic population due to the strong interaction between the atoms. However, these same interactions may lead to coherence-loss on atomic samples [14]. Such interaction can present either advantages or disadvantages in atomic systems, therefore they need to be well understood.

The dipole-dipole interaction is for sure the most important term involving two cold Rydberg atoms; and its importance has been recognized since the first experiments [15, 16]. However, the first experiment to observe evidence of its anisotropy, was carried out in 2004 by Carrol et al [17]. In this work, the authors have observed the electric field angular dependence of the dipole-dipole interaction in a quasi-unidimensional sample created by a confined laser beam geometry. Recently, Ravets and co-workers [18] have investigated the angular dependence of the dipole-dipole interaction in a much clearer system using two individual Rydberg atoms held in two microscopic optical dipole traps. Since their system is not an ensemble, the authors were able to obtain clearly the angular dependence of the dipole-dipole interaction.

Several research groups have been investigating, either theoretically or experimentally, highly interacting many-body unidimensional system using Rydberg atomic samples created by a confined laser beam geometry. Such works explore different aspects of condensed matter physics: i) transition to the crystalline phase [19, 20]; ii) energy transport [21]; iii) spatial correlations [22]; iv) Rydberg aggregates [23]; v) van der Waals interaction and Rydberg blockade effect [24–26]. Clearly, Rydberg

atoms can be used as a prototype for the study of such complex properties because they are a simpler system and easier to control. Besides, anisotropy effects may play an important role on such properties in a unidimensional sample.

In this work, we have observed the anisotropy of the dipole-dipole interaction by studying the Rydberg blockade effect in a tightly confined atomic sample held in a quasi-electrostatic trap (QUEST). The  $50S_{1/2}$  Rb Rydberg state population was measured as a function of ground state atoms density for several angles between the axis of the quasi-unidimensional sample and the orientation of an external dc electric field. We have demonstrated that the density limitation, imposed by Rydberg blockade effect, can be overcome by suppressing the dipole-dipole interaction in our sample. Besides, the unidimensionality of the sample was proved by using direct spatial ion imaging.

Our experiment starts with a magneto-optical trap (MOT), which operates in a stainless steel chamber with a background pressure below  $10^{-10}$  torr and it is loaded from an a rubidium 2DMOT. Such magneto-optical trap is used to load a quasi-electrostatic trap (QUEST), producing a non-polarized atomic sample of  $\sim 10^6$  atoms at a peak density of  $\approx 10^{12}$  atoms/cm<sup>3</sup> and temperature of 60  $\mu$ K. The QUEST is provided by a polarized 10.6  $\mu$ m CO<sub>2</sub> laser (COHERENT model GEM-100), which is focused into the MOT volume with a waist of 15  $\mu$ m and an available power of 80 W. More details on the experimental setup can be found in [27, 28]. In order to excite the  $50S_{1/2}$  state, we apply a laser pulse train, which are subsequently detected by pulsed-field ionization (PFI). This laser pulse train operates at 100 Hz for 1.5 s and it is composed of two narrow-bandwidth CW laser pulses near 780 nm and 480 nm, whose duration is about 1  $\mu$ s and have intensities of  $I_{780} = 1.6$  mW cm<sup>-2</sup> and  $I_{480} \approx 100$  W cm<sup>-2</sup> (Rabi frequency of 32 MHz). The 480 nm laser is stabilized in frequency using a commercial wavemeter (Highfinesse

model WS-7). All the electric fields are generated by a system of 8 independently-controlled electrodes, which are distributed in two aligned cloverleaf distribution sets, following the design of reference [29]. In the bottom electrodes of each set, we apply a  $5 \mu\text{s}$  PFI, which occurs 70 ns after the optical excitation. The electrons are detected using a microchannel plate detector (MCP), which gives an average of 300 Rydberg atoms per pulse at the highest atomic density and no electric field. The QUEST is turned off for about  $15 \mu\text{s}$  during the Rydberg excitation and detection to avoid any unwanted effects such as ac Stark shifts or photoionization of the Rydberg states [30]. During the laser pulse train the atomic population held in the QUEST decays, allowing us to study the  $50S_{1/2}$  Rydberg state population as a function of the ground state atomic density. In order to characterize the sample's decay, state-selective absorption imaging technique was used. The background electric field is estimated to be  $< 20 \text{ mV cm}^{-1}$ . A boxcar gate is used to selectively detect the  $50S_{1/2}$  population, a function of the ground state atomic density.

For  $nS$  states (in the absence of any dc electric field) the atoms interact only via van der Waals interaction, so the potential is purely repulsive and isotropic [31]. In the presence of an external field, the atoms become polarized and the interaction changes to an angular-dependent effective potential, given by:

$$V_{\text{eff}}(R, \theta) = \frac{C_6}{R^6} + \frac{C_3}{R^3}(1 - 3 \cos^2(\theta)) \quad (1)$$

where  $C_6$  is the van der Waals interaction parameter,  $C_3$  is the dipole-dipole interaction parameter ( $C_3 = |\mathbf{P}|^2/4\pi\epsilon_0$ , in S.I. units),  $\mathbf{P}$  is the electric dipole moment vector and  $\mathbf{R}$  is the internuclear separation vector. The effective potential is directly dependent on  $C_6$  and  $C_3$ , and  $C_3$  depends on the amplitude of the external electric field. By choosing the direction of such field, the effective potential can be either more repulsive, when the dipoles are parallel to each other, or less repulsive when the dipoles are aligned in a line. The first step in our experiment was to obtain a Stark spectrum, which was accomplished by locking the 480 nm laser at several detuning values ( $\Delta_{480}$ ) below the  $5P_{3/2}(F=4) \rightarrow 50S_{1/2}$  transition and scanning the dc electric field. Figure 1a shows a typical normalized  $50S_{1/2}$  population as a function of the dc field for  $\Delta_{480} = 151 \text{ MHz}$ . By combining similar spectrum for different  $\Delta_{480}$ , we can obtain the Stark spectrum (Fig. 1b). We have chosen to excite the atoms in the  $50S_{1/2}$  state between the 3<sup>rd</sup> and 4<sup>th</sup> avoided-crossings with the manifold hydrogenic lines at a field of  $2.37 \text{ V cm}^{-1}$ . At this condition, the dipole-dipole interaction strength is comparable to the van der Waals interaction at the highest achievable experimental density.

To guarantee that the applied field is behaving as expected, the electrodes were calibrated by taking several Stark maps near the  $50S_{1/2}$  state and comparing it to the theoretical value on each direction  $X$ ,  $Y$  and  $Z$  in-

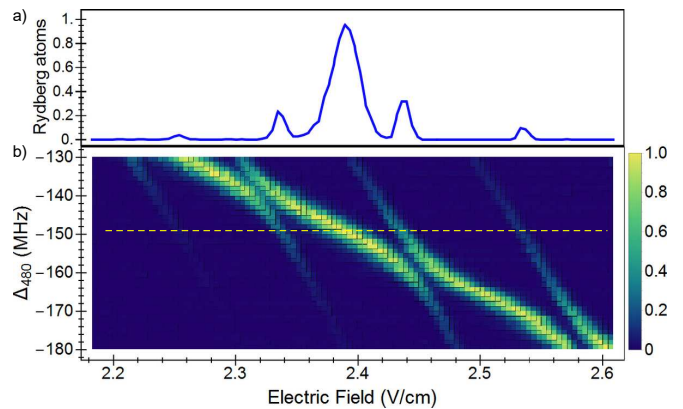


FIG. 1. (Color online) a) Normalized  $50S_{1/2}$  population as a function of the dc electric field for  $\Delta_{480} = 150 \text{ MHz}$ . b) Experimental Stark spectrum showing the avoided-crossings of the  $50S_{1/2}$  state with the manifold hydrogenic lines. This map shows our capability to resolve the avoided-crossings of interest. The yellow line marks the position of the excitation frequency for the experiment.

dependently, following the procedure described in [29]. This procedure allows us to obtain the zero field position and calibration factor simultaneously for each coordinate. Then, before each Rydberg blockade measurement at a given angle, we performed a field scan to check the position of the chosen resonance. By setting the field at the resonance (as shown in fig. 1a), we can guarantee the amplitude of the field for all angles within  $20 \text{ mV cm}^{-1}$ . As the angle was varied, the voltages applied in the electrodes presented small variations in order to keep the resonance. By computational simulations, we were able to estimate that such voltage variations represent an angle error that is less than  $4^\circ$ .

Figure 2 shows the  $50S_{1/2}$  state population as a function of ground state atoms density for several field orientation at an amplitude of  $2.38 \text{ V cm}^{-1}$  and  $\Delta_{480} = 151 \text{ MHz}$ . Each point is an average of 40 independent measurements, and the error bars were suppressed to simplify the graph; however they are on the order of 15%. The Rydberg population is normalized for the saturated value of final population at zero field. The trap is formed along the  $Y$  axis and the angle is defined by the orientation of the applied electric field and the trap axis, on the plane  $YZ$ . For comparison we also show the measurement at zero field and for the field applied at the magic angle ( $\theta = 54.7^\circ$ ).

It is important to notice that the final population varies around the zero field population as the angle is changed. It is also clear that the final population at the magic angle is almost the same as the population in the zero field condition; indicating that one can suppress the dipole-dipole interaction in our sample. We should point out that the behavior of these two curves (no electric field and field at the magic angle), in the low density regime, is slightly different. We believe that at low density, the sample does not behave as a quasi-unidimensional en-

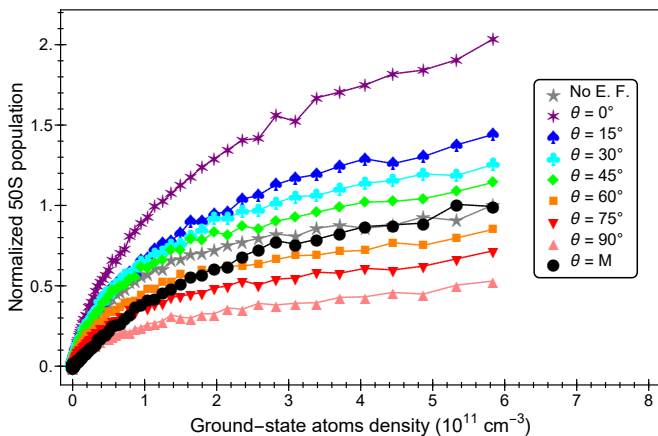


FIG. 2. (Color online)  $50S_{1/2}$  state population as a function of ground state atoms density for several field orientation for an amplitude of  $2.38 \text{ V cm}^{-1}$  and  $\Delta_{480} = 151 \text{ MHz}$ .

semble, therefore, there will be differences between the zero field and the magic angle signal respectively. As the density increases, and the sample reaches the blocked regime, its unidimensionality rises leading to a preferential axis for the atomic distribution and, consequently, to no differences on the final population.

In order to demonstrate that such result is consistent with Rydberg atom blockade, we have applied a classical hard sphere model in the steady state [32, 33]. This is one of the simplest model available in the literature, but it does contain the main physical insights and correctly describes the effect. Briefly, the hard sphere model treats Rydberg atoms as hard spheres with a radius equal to the blockade radius ( $R_{bl}$ ), thereby defining an exclusion volume around each excited atom. In the blockade regime, the excitation volume is assumed to be densely packed by these spheres so that information about the excited state population is obtained. The blockade radius is an important parameter in such model, and it can be obtained by imposing that the laser bandwidth ( $\Gamma$ ) matches the effective potential at the interatomic distance  $R_{bl}$ :

$$\Gamma = \frac{C_6}{R_{bl}^6} + \frac{C_3}{R_{bl}^3}(1 - 3 \cos^2(\theta)) \quad (2)$$

From Eq. 2, it is clear that the blockade radius is now angular dependent, therefore the final Rydberg population should vary depending on the field orientation. In order to compare the experimental angular dependence of the  $50S_{1/2}$  population with the blockade hard sphere model, we plot the average final number of Rydberg atoms as a function of the electric field angle; which is shown in figure 3. Each point is an average of the last three experimental points, at the highest atomic density, of each curve from figure 2 and their standard deviations is used as error bars.

The line is a fitting using the hard sphere model, from where we obtained the following interaction parameters:

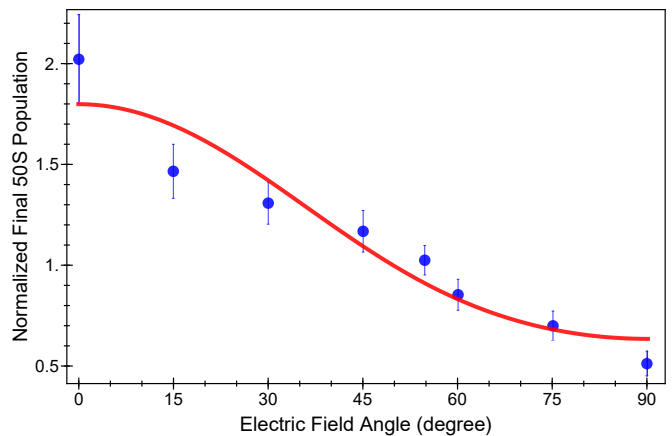


FIG. 3. (Color online)  $50S$  state population as a function of angle for the highest atomic ground state density for an amplitude of  $2.38 \text{ V cm}^{-1}$ . The line is the theoretical prediction using the hard sphere model [32, 33].

$C_6 = 18418 \text{ MHz } \mu\text{m}^6$  and  $C_3 = 99.74 \text{ MHz } \mu\text{m}^3$ . The obtained  $C_6$  is close to the theoretical one for the  $50S_{1/2}$  state ( $15296 \text{ MHz } \mu\text{m}^6$ ) [34]. The obtained  $C_3$  is about seven times larger than the theoretical one ( $14.375 \text{ MHz } \mu\text{m}^3$ ), which is calculated in the asymptotic regime, using the atomic dipole moment. Such difference is not surprising, and it may be due to two factors:

- i) The interaction between two Rydberg atoms is more complex than this simplistic potential based on the interaction parameter, obtained from the single-atom Stark effect, which is expected to be valid only at long range and not at the blocked regime. In a recent work, we have shown that the multilevel character of the interaction due to the presence of high angular momentum states is crucial for the calculation of accurate potential curves and interpretation of Rydberg interaction experiments[28]. Such calculation requires to consider all  $L$  states up to  $L = (n-1)$  for at least two manifolds above and below the state of interest. Since in this experiment  $n = 50$ , such calculation is more difficult and challenging than in our previous work[28], and it is under implementation[35].
- ii) The hard sphere blockade model is a very simple one and it does deviate from the experiment results at higher densities. We have observed in a previous work, that while the model saturates at high density, the experimental Rydberg atomic population still presents a slow increase[27]

To explore the capability of nullifying the dipole-dipole interactions, in another experiment, we have measured the  $50S_{1/2}$  population as a function of the ground state atomic density for several electric fields at the magic angle. The electric field amplitudes are chosen between the different avoided-crossings of the  $50S_{1/2}$  with the manifold hydrogenic lines. Different field amplitudes lead to a change in the interaction strength and consequently the final population of Rydberg atom. But as we have shown before, at the magic angle the dipole-dipole interaction

is suppressed and, therefore the curves should be independent of the field amplitude. This can be observed in figure 4. Here we present saturation curves for different field amplitudes at the magic angle. The inset shows the standard deviation from the average for all curves, which has a maximum of 8% indicating that the curves are independent from the electric field amplitude.

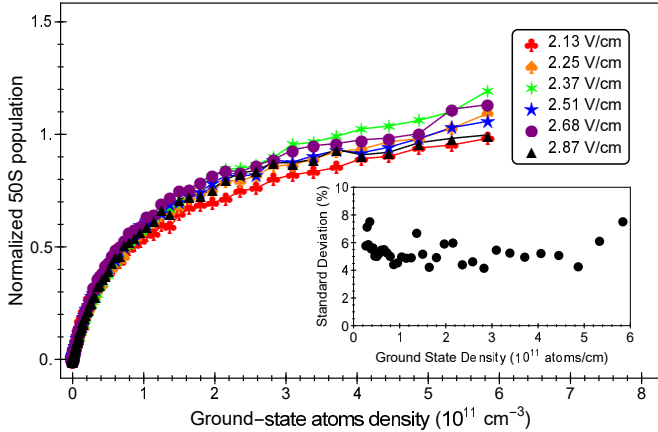


FIG. 4. (Color online)  $50S_{1/2}$  state population as a function of the ground state atomic density for several electric fields at the magic angle.

Although the Rydberg sample behaves as 1D, we have no other evidence that in fact it may be consider like one. In order to clarify this issue, we have performed a spatially resolved single-atom ion imaging of our Rydberg sample. The ion imaging system is composed of: i) a magnifying electrostatic lens, positioned perpendicularly to the electrodes system and axially aligned with the ion path to the detector, whose magnification depends on the applied voltage; ii) a grounded tube of flight of 15 cm; iii) a spatially sensitive ion detector (BOS-18-OPT01 from Beam Imaging Solutions), which consists of two MCP coupled to a phosphor screen; and iv) a triggerable digital camera, which captures the images outside the vacuum system. Our system, and its operation, is very similar to other reported systems in the literature [36, 37]. To characterize the sample we begin by taking  $\approx 3000$  images from the MCP detector; each image shows the ion impact positions for a single excitation pulse (780 nm and 480 nm laser pulses) at the highest atomic density of the each QUEST sample. Figure 5 (a) shows the sum of about 3000 ion images in a normalized colorscale at zero field excitation. By calculating the paircorrelation function (PCF), using the same procedure established by Schwarzkopf and co-workers [36], we can obtain the sum of all PCF, presented in figure 5 (b). In this figure, one can notice an anisotropic structure around the origin; which we have observed that it is independent either of electric field amplitude or direction. One feature of such structure is locate along the X axis ( $+X$  and  $-X$ ), and it represents the probability of having two Rydberg atoms interacting with each along the

X axis (radial axis of the sample), which is very small for our system. In fact, most of the interaction between two Rydberg atoms happens along the sample's axis (Y axis), with an angle that is less than  $\theta = 4.5^\circ$ . Considering the Rydberg atoms as hard spheres, the maximum classical impact parameter possible in our sample is  $2R_{bl} \sin(4.5^\circ) \approx 0.8 \mu\text{m}$ . This clearly demonstrates that our sample is quasi-unidimensional, and the atoms are almost aligned in a single line.

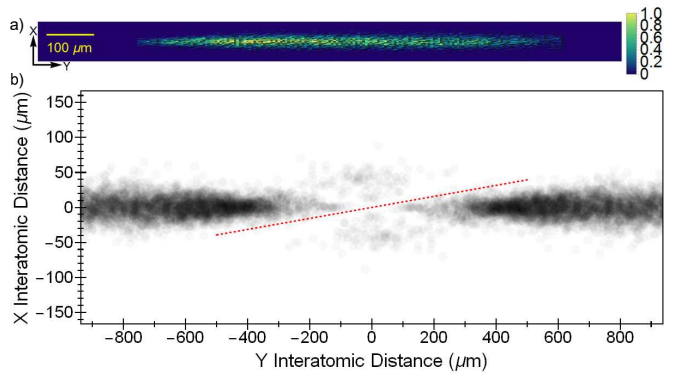


FIG. 5. (Color online) a) sum of 3000 ion images for  $\mathbf{E} = 2.38 \hat{y} \text{ V/cm}$ . b) Sum of all paircorrelations where we can observe a structure at the center. The red-dashed line is plotted with  $4.5^\circ$  related to the sample axis (Y). Here is important to notice that the x and y scales are not the same.

In summary, we have demonstrated that a tightly confined atomic sample held in a quasi-electrostatic trap (QUEST) behaves as an unidimensional sample for cold Rydberg atom experiments. In such system, we were able to measure directly the angular dependence of the dipole-dipole interaction and demonstrated that it becomes stronger when the atomic induced-dipole-moments are aligned  $\theta = 90^\circ$  with respect the sample axis, leading to a super-blockaded sample. And on the other hand, if the field is aligned  $\theta = 0^\circ$ , the effective potential is smaller, leading to an enhanced final population of Rydberg atoms. We have also demonstrated that at the magic angle  $\theta = 54.7^\circ$  the dipole-dipole interaction is suppressed, leading the sample of Rydberg atoms to behave, in the presence of electric field, in the same way as the field free case. The unidimensionality of our sample was verified by a spatially resolved ion imaging method, corroborating our dipole-dipole interaction results.

Such results may have several implications on cold Rydberg atom experiment. For example, overcoming the density limitation of Rydberg atoms may be important for time dependent experiments where the direction of the field can be changed suddenly, taking the system from a low interacting condition to a high interacting regime. That may be useful for the study of many-body effects in a strongly-coupled systems in condensed matter physics [19–21, 23]. The suppression of the dipole-dipole interaction at the magic angle is also very significant because allows one to perform experiments where

high order interactions may be investigated in more details, for instance dipole-quadrupole, extracting information of intrinsic properties of interatomic potentials that were previously unachievable. Besides, the presence of an external field, at the magic angle, could also allow the excitation of states, which are not dipole allowed, like  $nP$

and  $nF$ , with comparable conditions to a field-free case.

## I. ACKNOWLEDGMENTS

This work is supported by grants 2011/22309-8 and 2013/02816-8, São Paulo Research Foundation (FAPESP), U.S. Army Research Office (grant W911NF-15-1-0638) and CNPq.

- 
- [1] M. P. Jones, L. G. Marcassa, and J. Shaffer, *Journal of Physics B: Atomic, Molecular and Optical Physics* **48**, 180201 (2015).
  - [2] L. G. Marcassa and J. P. Shaffer, in *Advances in Atomic, Molecular and Optical Physics*, Advances In Atomic, Molecular, and Optical Physics, Vol. 63, edited by E. Arimondo, P. R. Berman, and C. C. Lin (Academic Press, 2014) p. 47.
  - [3] T. F. Gallagher and P. Pillet, in *Advances in Atomic, Molecular and Optical Physics*, Advances In Atomic, Molecular, and Optical Physics, Vol. 56, edited by E. Arimondo, P. R. Berman, and C. C. Lin (Academic Press, 2008) p. 161.
  - [4] V. A. Nascimento, L. L. Caliri, A. Schwettmann, J. P. Shaffer, and L. G. Marcassa, *Phys. Rev. Lett.* **102**, 213201 (2009).
  - [5] J. S. Cabral, J. M. Kondo, L. F. Gonçalves, V. A. Nascimento, L. G. Marcassa, D. Booth, J. Tallant, A. Schwettmann, K. R. Overstreet, J. Sedlacek, and J. P. Shaffer, *J. Phys. B* **44**, 184007 (2011).
  - [6] D. Booth, S. T. Rittenhouse, J. Yang, H. R. Sadeghpour, and J. P. Shaffer, *Science* **348**, 99 (2015), <http://science.sciencemag.org/content/348/6230/99.full.pdf>.
  - [7] L. Béguin, A. Vernier, R. Chicireanu, T. Lahaye, and A. Browaeys, *Phys. Rev. Lett.* **110**, 263201 (2013).
  - [8] A. Browaeys, D. Barredo, and T. Lahaye, *Journal of Physics B: Atomic, Molecular and Optical Physics* **49**, 152001 (2016).
  - [9] M. Saffman, T. G. Walker, and K. Mølmer, *Rev. Mod. Phys.* **82**, 2313 (2010).
  - [10] I. Lesanovsky and J. P. Garrahan, *Phys. Rev. Lett.* **111**, 215305 (2013).
  - [11] D. Tong, S. M. Farooqi, J. Stanojevic, S. Krishnan, Y. P. Zhang, R. Côté, E. E. Eyler, and P. L. Gould, *Phys. Rev. Lett.* **93**, 063001 (2004).
  - [12] K. Singer, M. Reetz-Lamour, T. Amthor, L. G. Marcassa, and M. Weidemüller, *Phys. Rev. Lett.* **93**, 163001 (2004).
  - [13] D. Comparat and P. Pillet, *J. Opt. Soc. Am. B* **27**, A208 (2010).
  - [14] M. Hoening, W. Abdussalam, M. Fleischhauer, and T. Pohl, *Phys. Rev. A* **90**, 021603 (2014).
  - [15] W. R. Anderson, J. R. Veale, and T. F. Gallagher, *Phys. Rev. Lett.* **80**, 249 (1998).
  - [16] I. Mourachko, D. Comparat, F. de Tomasi, A. Fioretti, P. Nosbaum, V. M. Akulin, and P. Pillet, *Phys. Rev. Lett.* **80**, 253 (1998).
  - [17] T. J. Carroll, K. Claringbould, A. Goodsell, M. J. Lim, and M. W. Noel, *Phys. Rev. Lett.* **93**, 153001 (2004).
  - [18] S. Ravets, H. Labuhn, D. Barredo, T. Lahaye, and A. Browaeys, *Phys. Rev. A* **92**, 020701 (2015).
  - [19] M. Hönig, D. Muth, D. Petrosyan, and M. Fleischhauer, *Phys. Rev. A* **87**, 023401 (2013).
  - [20] P. Schauß, J. Zeiher, T. Fukuhara, S. Hild, M. Cheneau, T. Macrì, T. Pohl, I. Bloch, and C. Gross, *Science* **347**, 1455 (2015), <http://science.sciencemag.org/content/347/6229/1455.full.pdf>.
  - [21] D. W. Schönleber, A. Eisfeld, M. Genkin, S. Whitlock, and S. Wüster, *Phys. Rev. Lett.* **114**, 123005 (2015).
  - [22] C. Ates and I. Lesanovsky, *Phys. Rev. A* **86**, 013408 (2012).
  - [23] H. Schempp, G. Günter, M. Robert-de Saint-Vincent, C. S. Hofmann, D. Breyel, A. Komnik, D. W. Schönleber, M. Gärttner, J. Evers, S. Whitlock, and M. Weidemüller, *Phys. Rev. Lett.* **112**, 013002 (2014).
  - [24] N. Thaicharoen, A. Schwarzkopf, and G. Raithel, *Phys. Rev. A* **92**, 040701 (2015).
  - [25] M. M. Valado, C. Simonelli, M. D. Hoogerland, I. Lesanovsky, J. P. Garrahan, E. Arimondo, D. Ciampini, and O. Morsch, *Phys. Rev. A* **93**, 040701 (2016).
  - [26] R. Faoro, C. Simonelli, M. Archimi, G. Masella, M. M. Valado, E. Arimondo, R. Mannella, D. Ciampini, and O. Morsch, *Phys. Rev. A* **93**, 030701 (2016).
  - [27] J. M. Kondo, L. F. Gonçalves, J. S. Cabral, J. Tallant, and L. G. Marcassa, *Phys. Rev. A* **90**, 023413 (2014).
  - [28] J. M. Kondo, D. Booth, L. F. Gonçalves, J. P. Shaffer, and L. G. Marcassa, *Phys. Rev. A* **93**, 012703 (2016).
  - [29] R. Löw, U. Raitzsch, R. Heidemann, V. Bendkowsky, B. Butscher, A. Grabowski, and T. Pfau, arXiv preprint arXiv:0706.2639 (2007).
  - [30] J. Tallant, D. Booth, and J. P. Shaffer, *Phys. Rev. A* **82**, 063406 (2010).
  - [31] T. G. Walker and M. Saffman, *Phys. Rev. A* **77**, 032723 (2008).
  - [32] M. Robert-de Saint-Vincent, C. S. Hofmann, H. Schempp, G. Günter, S. Whitlock, and M. Weidemüller, *Phys. Rev. Lett.* **110**, 045004 (2013).
  - [33] C. Ates, S. Sevinçli, and T. Pohl, *Phys. Rev. A* **83**, 041802 (2011).
  - [34] A. Reinhard, T. C. Liebisch, B. Knuffman, and G. Raithel, *Phys. Rev. A* **75**, 032712 (2007).
  - [35] J. P. Shaffer, (private communication).
  - [36] A. Schwarzkopf, R. E. Sapiro, and G. Raithel, *Phys. Rev. Lett.* **107**, 103001 (2011).
  - [37] D. P. Fahey, T. J. Carroll, and M. W. Noel, *Phys. Rev. A* **91**, 062702 (2015).